

## Electronic Supplementary Information:

# Gold Nanoparticle Superlattices: Correlating Chemiresistive Responses with Analyte Sorption and Swelling

*Natalia Olichwer, Andreas Meyer, Mazlum Yesilmen and Tobias Vossmeier\**

Institute of Physical Chemistry, University of Hamburg, Grindelallee 117, 20146 Hamburg,  
Germany

### **Corresponding Author**

\*E-mail: tobias.vossmeier@chemie.uni-hamburg.de

## 1. Preparation of GNP superlattice films and structural characterization

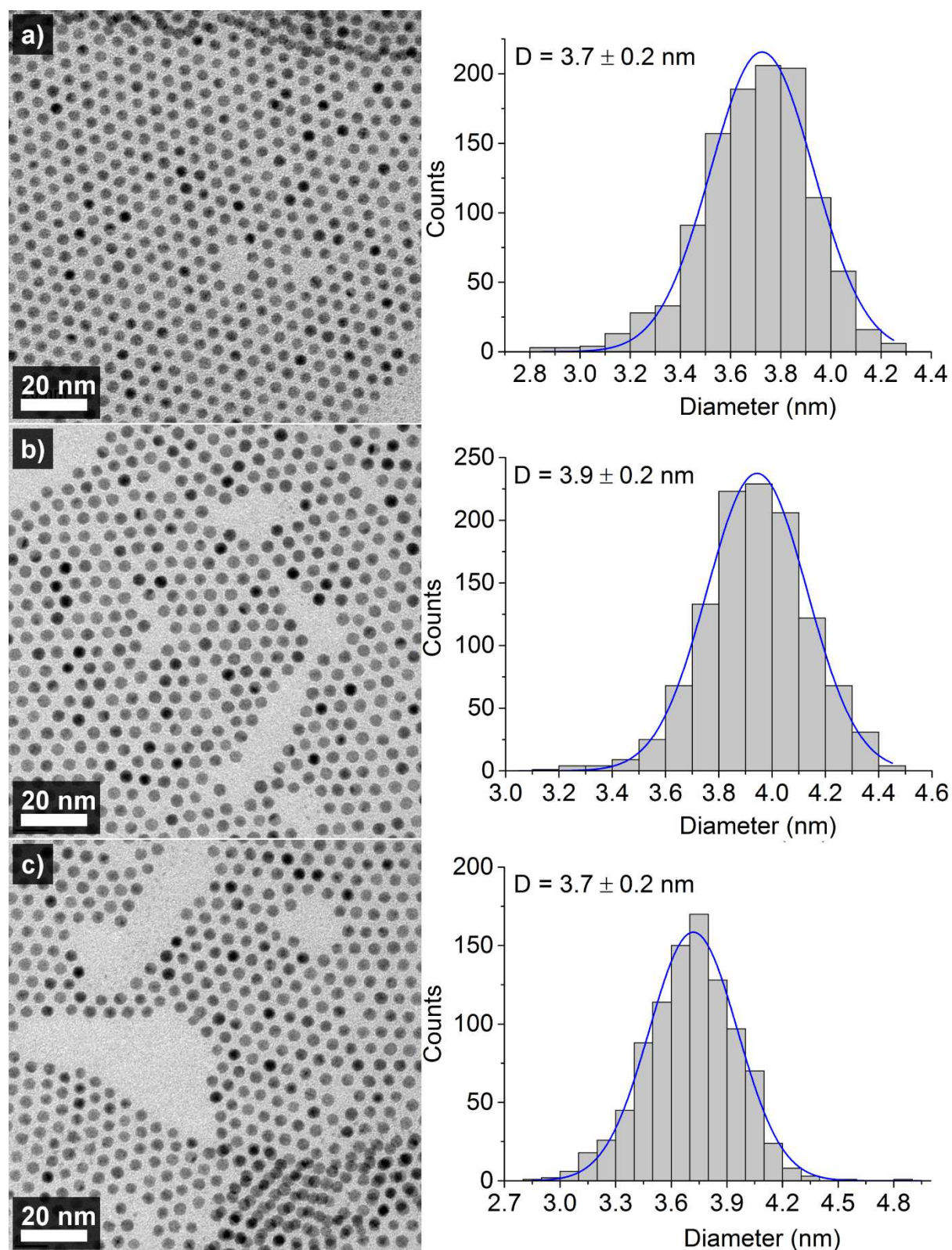
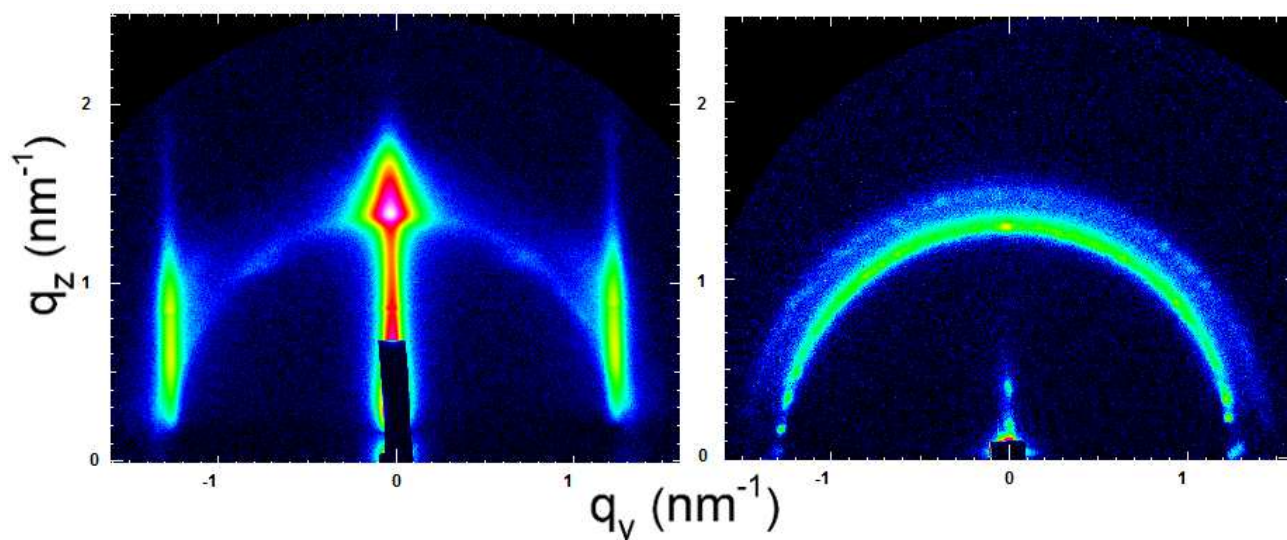


Figure S1: TEM-images and size histograms of samples a) GNP1, b) GNP2 and c) GNP3.



**Figure S2:** GISAXS patterns of GNP superlattice films prepared from samples GNP1 (left) and GNP3 (right). The film prepared from sample GNP3 was significantly thicker ( $\sim 500$  nm) than those from samples GNP1 and GNP2 ( $\sim 100$  nm). Thus, the GISAXS pattern shown on the right is strongly dominated by the SAXS signature.

### GISAXS analysis

As mentioned in the main document the GNP core diameters obtained from SAXS analyses tend to be larger compared to the diameters obtained by TEM measurements. To explain this deviation it should be taken into account that the gold core diameters extracted from the SAXS analysis are significantly influenced by the ratio of the signal intensities of the (111)- and (200)-reflections, as indicated in Figure S3. Because this ratio is influenced by preferred orientations of supercrystalline domains, we attribute the observed differences of TEM- and GISAXS-measured gold core sizes to such texturing effects. The SEM-image of sample GNP2 presented in Figure S5 indicates a preferential orientation of the (111)-planes parallel to the substrate surface. Additionally, we cannot exclude that a minor fraction of our particle films crystallized as bcc superlattice. Because the (110)-bcc reflection would overlap with the (111)-fcc reflection this reflection would be intensified relative to the (200)-fcc reflection and, thus, the extracted gold core size would become larger. However, as shown by Figure S4, we

did not detect the bcc (200)-reflection, which would be expected at  $q \sim 1.8 \text{ nm}^{-1}$ . Thus, there is no indication for the presence of significant amounts of the bcc superlattice.

Because the SAXS analysis did not allow us to correct the extracted GNP core diameters for the effects discussed above, we used the center-to-center distance observed by GISAXS, but the GNP core diameters measured by TEM. Figure S3 shows the measured and calculated scattering curves of the superlattice film prepared from sample GNP2. As indicated, the TEM-measured radius of 1.95 nm was used to generate one of the calculated curves, while using the radius of 2.4 nm generated the best match with the SAXS curve. Among the three GNP samples used in our *in situ* GISAXS/chemiresistor study sample GNP2 showed the largest deviation of GNP core sizes obtained by the two methods. However, from Figure S3 it is evident that the (111)- and (200)-fcc peak positions of the calculated curves and, thus, the extracted center-to-center distances between neighboring particles are essentially independent of the GNP core size.

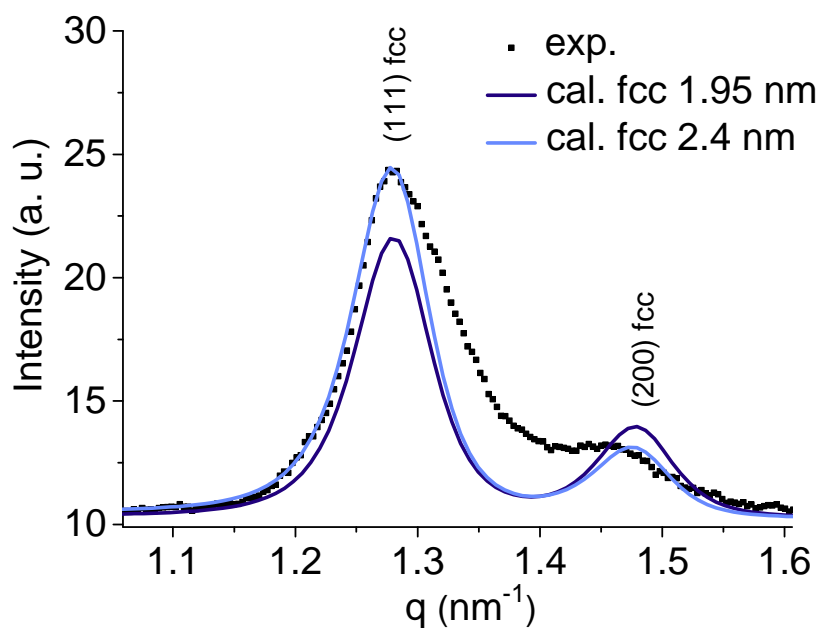


**Figure S3:** SAXS curve extracted from the GISAXS pattern of a GNP superlattice film prepared from sample GNP2 (black dots) and calculated SAXS curves using a GNP core radius of 2.4 nm (light blue line) and the GNP core radius of 1.95 nm obtained from TEM images (dark blue line). The position of the reflections of the two calculated SAXS curves remains essentially unaffected when altering GNP core size.

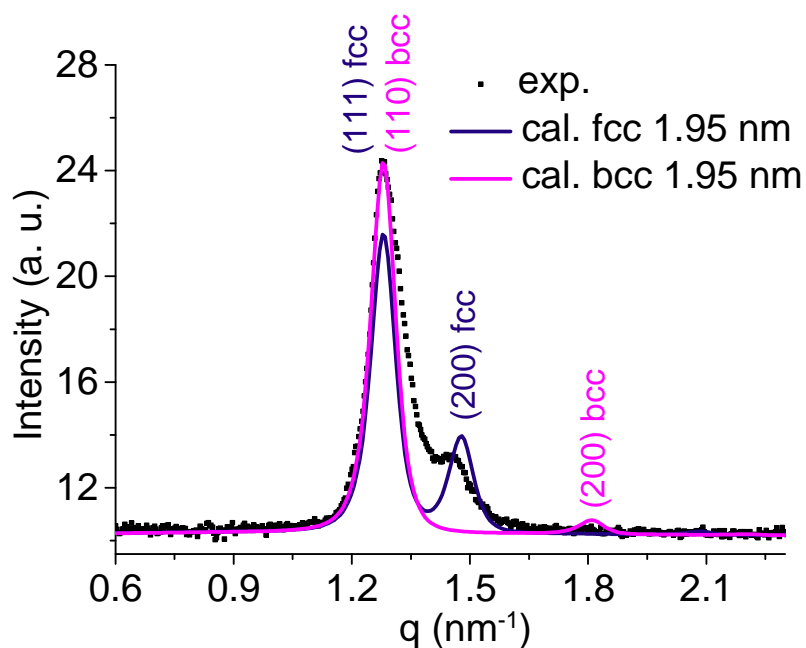


**Figure S4:** SAXS curve extracted from the GISAXS pattern of a GNP superlattice film prepared from sample GNP2 (black dots) and calculated curves for fcc (dark blue line) and bcc (magenta line) superlattices using the TEM-measured GNP core radius, as indicated.

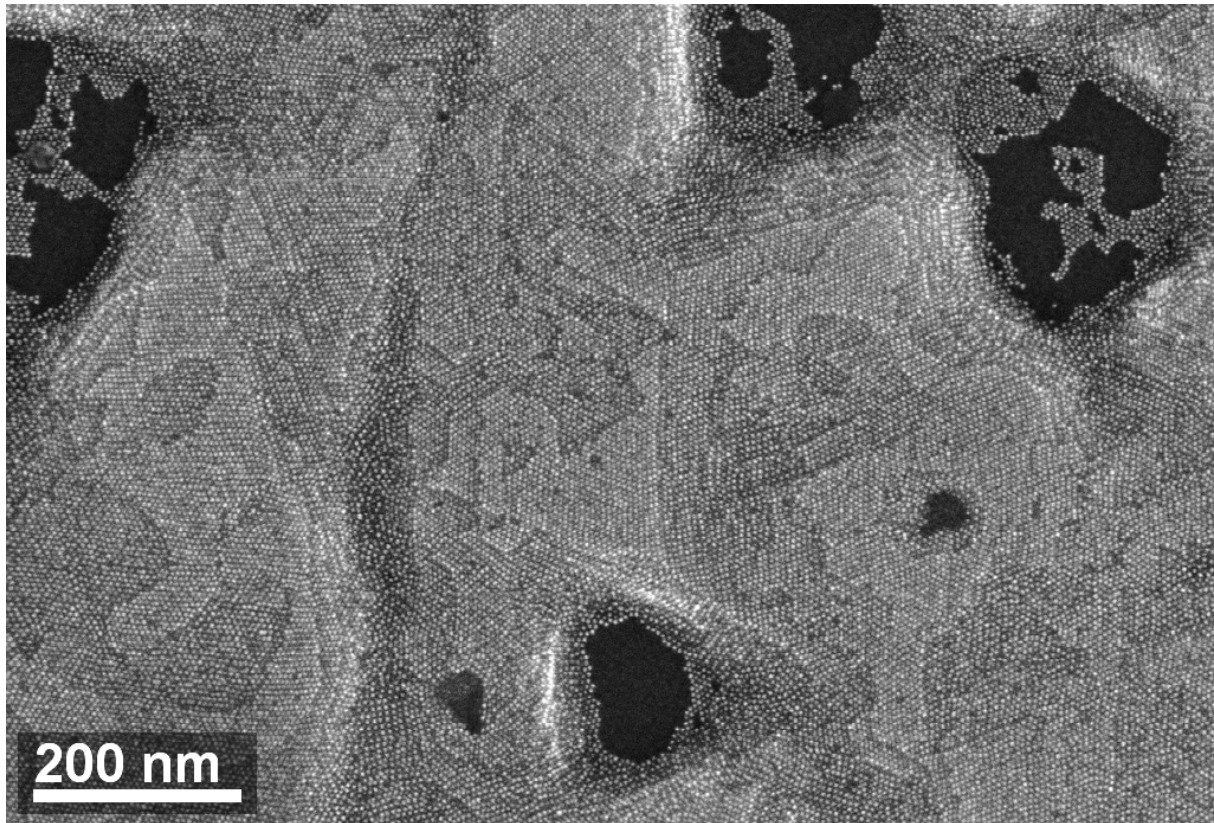


**Figure S5:** SEM-image of a GNP superlattice film prepared from sample GNP2 showing the (111) planes oriented parallel to the surface of the silicon substrate.

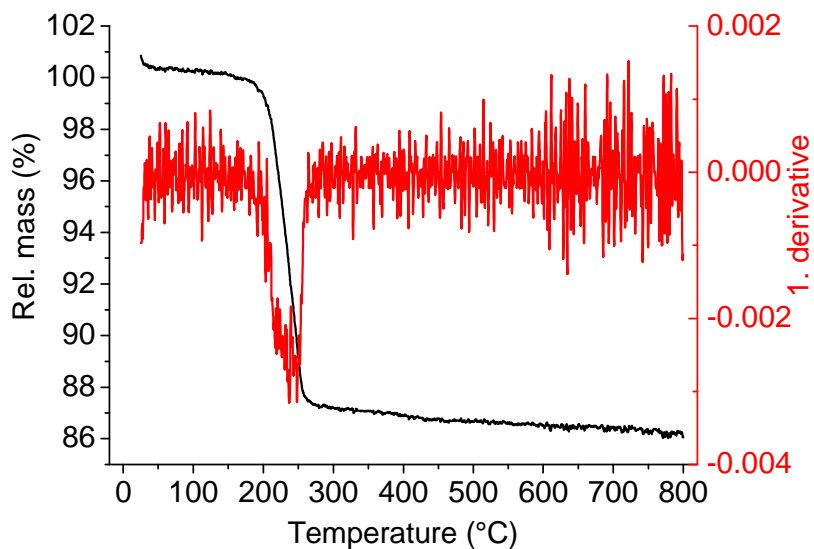


**Figure S6:** Thermogravimetric analysis (TGA) of sample GNP2. A comparison of the gold mass fraction of a GNP superlattice determined by TGA and calculated based on TEM and GISAXS data is provided in Table S1 for two GNP samples.

**Table S1:** Mass fraction of gold  $n_{Au}$  derived from the superlattice model based on TEM and GISAXS data and  $n_{Au,TGA}$  determined by TGA for samples GNP2 (TGA data are shown in Figure S6) and GNP4. The GNP core diameter  $D$  was measured by TEM whereas the edge-to-edge distance  $\Delta\delta$  between neighboring GNP cores was calculated by subtracting  $D$  from the GISAXS-measured center-to-center distance. The calculation of  $n_{Au}$  values is detailed in Section 3 of the ESI.

Sample	$D$ (nm)	$\delta$ (nm)	$n_{Au,TGA}$ (%)	$n_{Au}$ (%)
GNP2	3.9	2.1	85.5	86.5
GNP4	3.8	1.9	86.2	86.1

## 2. GNP Superlattice films dosed with solvent vapors: sorption, swelling and chemiresistive responses

### 2.1 Vapor sorption in GNP superlattice films measured by microgravimetry (QCM)

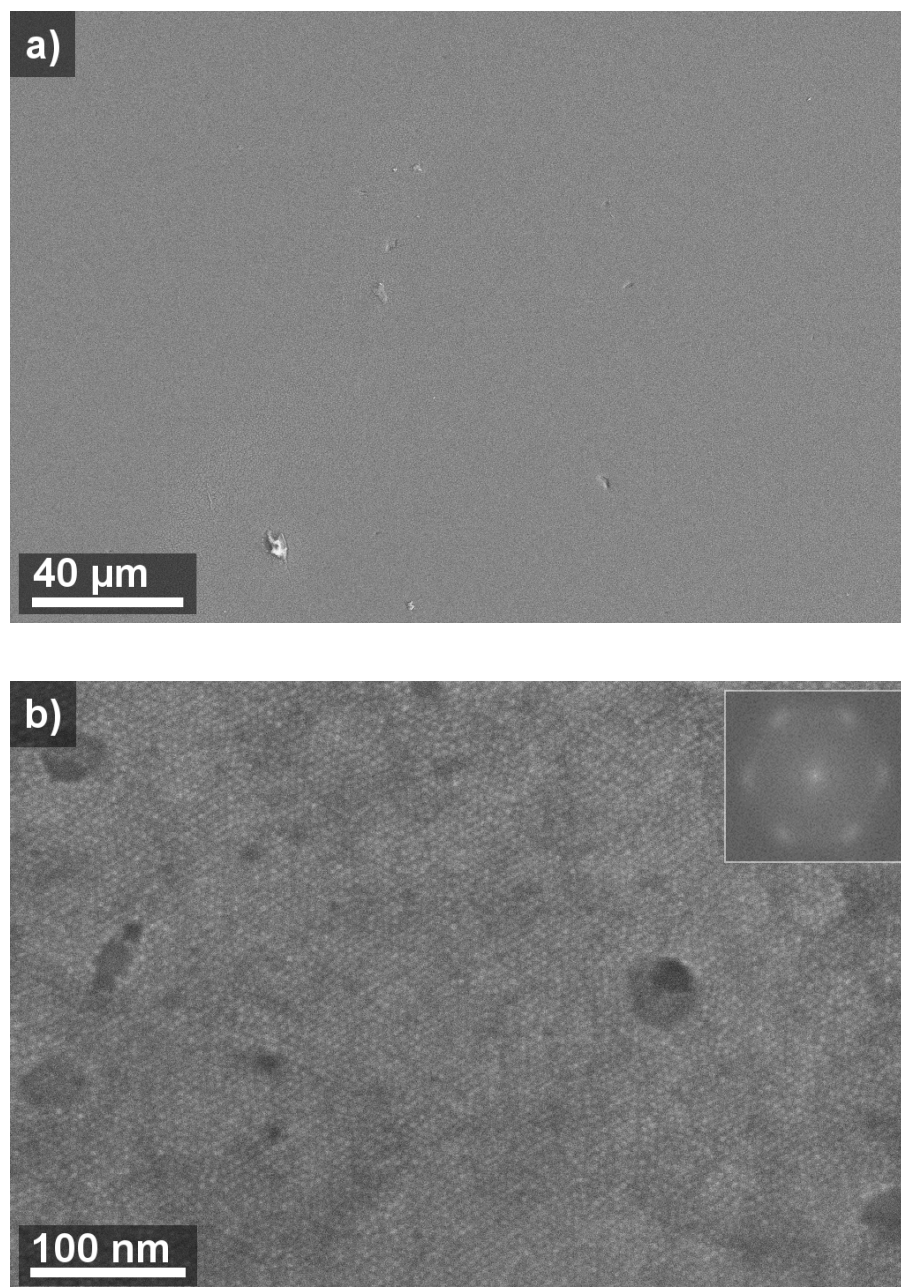


**Figure S7:** a) SEM overview image of a GNP superlattice film deposited onto the gold electrode of a QCM sensor. b) High resolution SEM image and its Fourier transform.

## 2.2 Sorption-induced swelling of GNP superlattice films measured by *in situ* GISAXS

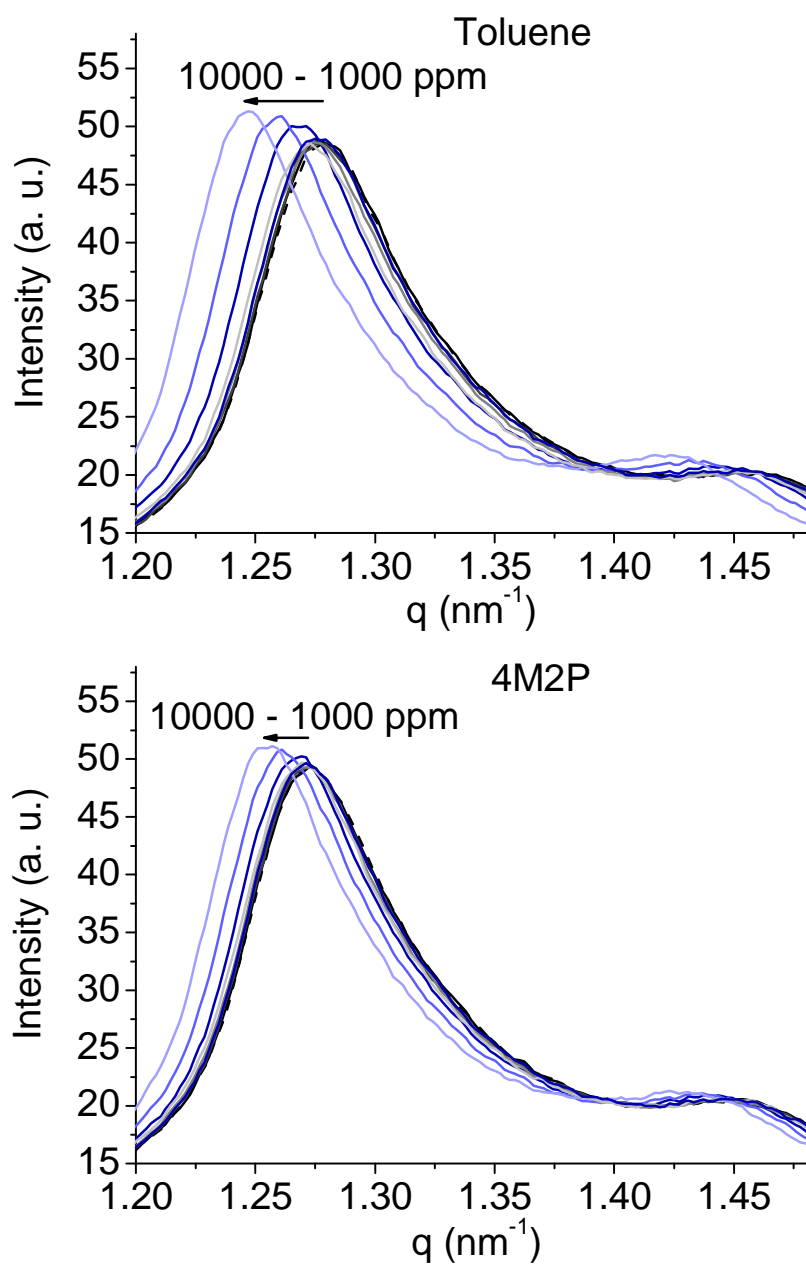


**Figure S8:** SAXS curves of a GNP film (sample GNP3) dosed with toluene (top) and 4M2P (bottom) vapors at different concentrations (1000, 4000, 7000, 10000 ppm, blue lines) and when purged with nitrogen between vapor exposures (black to grey lines). The data demonstrate that sorption-induced swelling was essentially reversible.

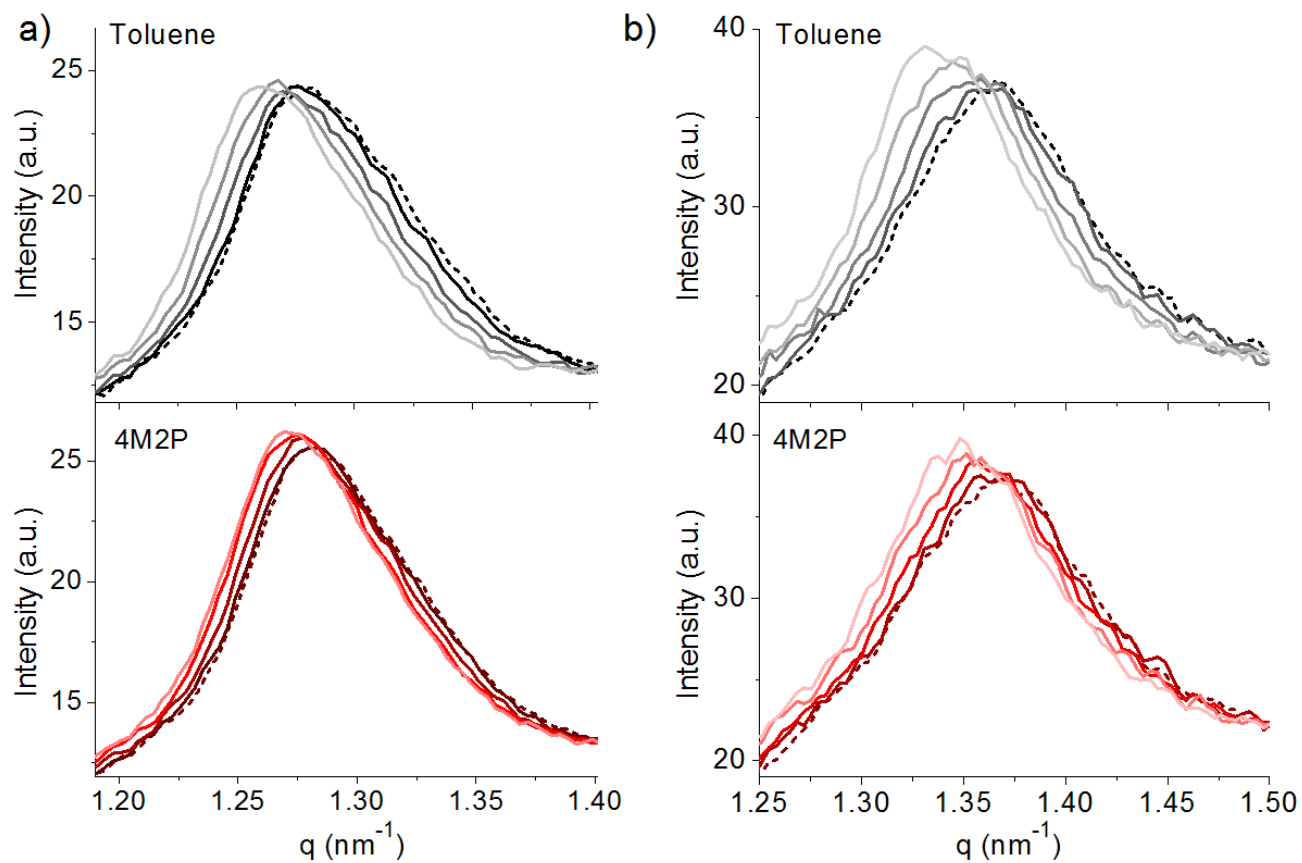


**Figure S9:** GISAXS-measured (111)-reflection of GNP superlattice films, prepared from samples GNP2 (a) and GNP1 (b), under nitrogen (dotted lines) and during exposure to vapors of toluene (black) and 4M2P (red). The increase in concentration (1000, 4000, 7000, 10000 ppm) is indicated by using dark to light colored graphs. The corresponding scattering patterns are shown in Figure 2 (main document) and Figure S2.

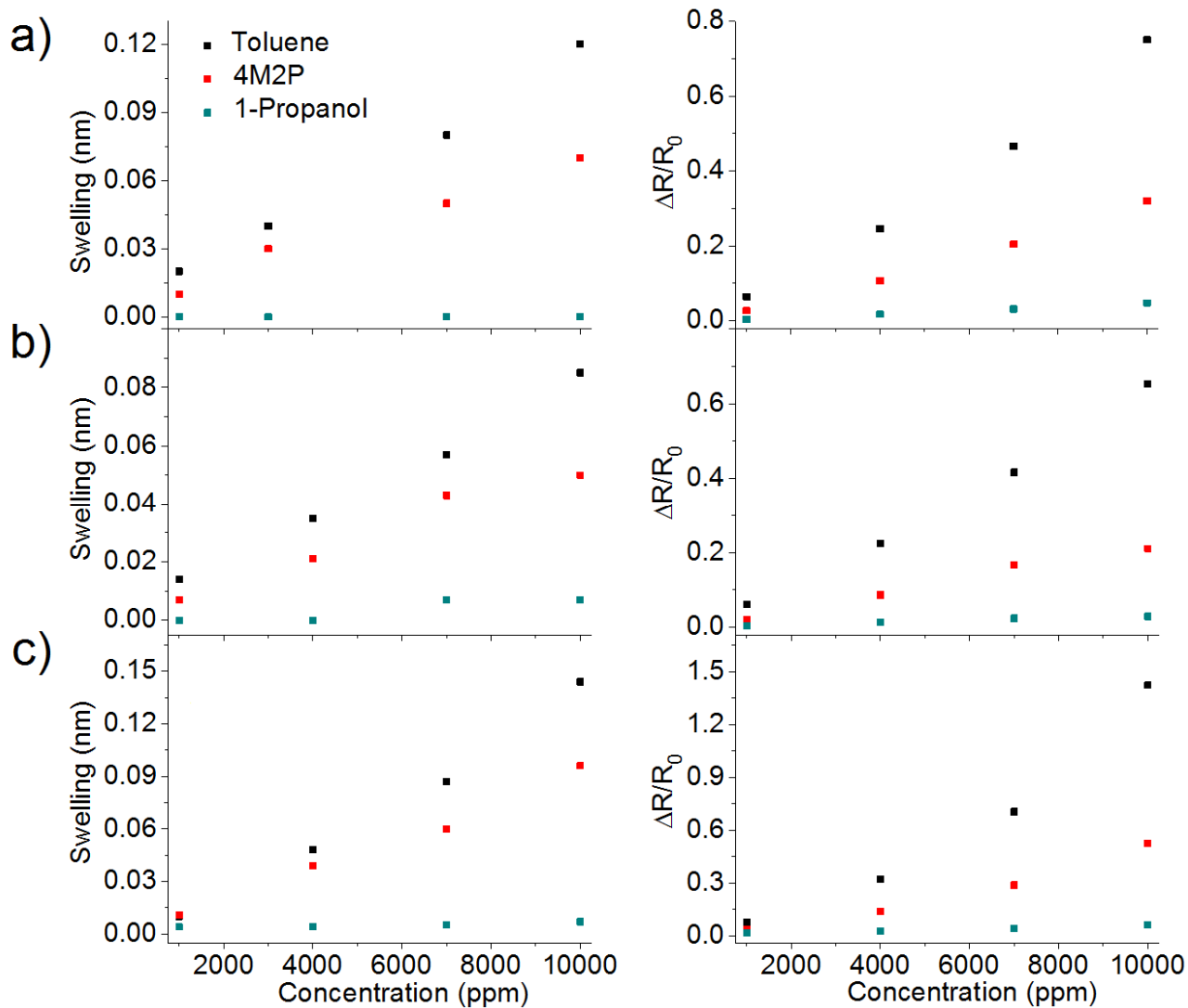


**Figure S10:** Interparticle distance changes  $\Delta\delta$  (left) and chemiresistive responses (right) as a function of applied vapor concentrations for GNP superlattice films prepared from samples a) GNP1, b) GNP2, and c) GNP3. Mean values of the interparticle distance changes and chemiresistive responses are shown in Figures 6 and 11 of the main document and Figure S13, respectively.

## 2.3 Sorption-induced chemiresistive responses of GNP superlattice films

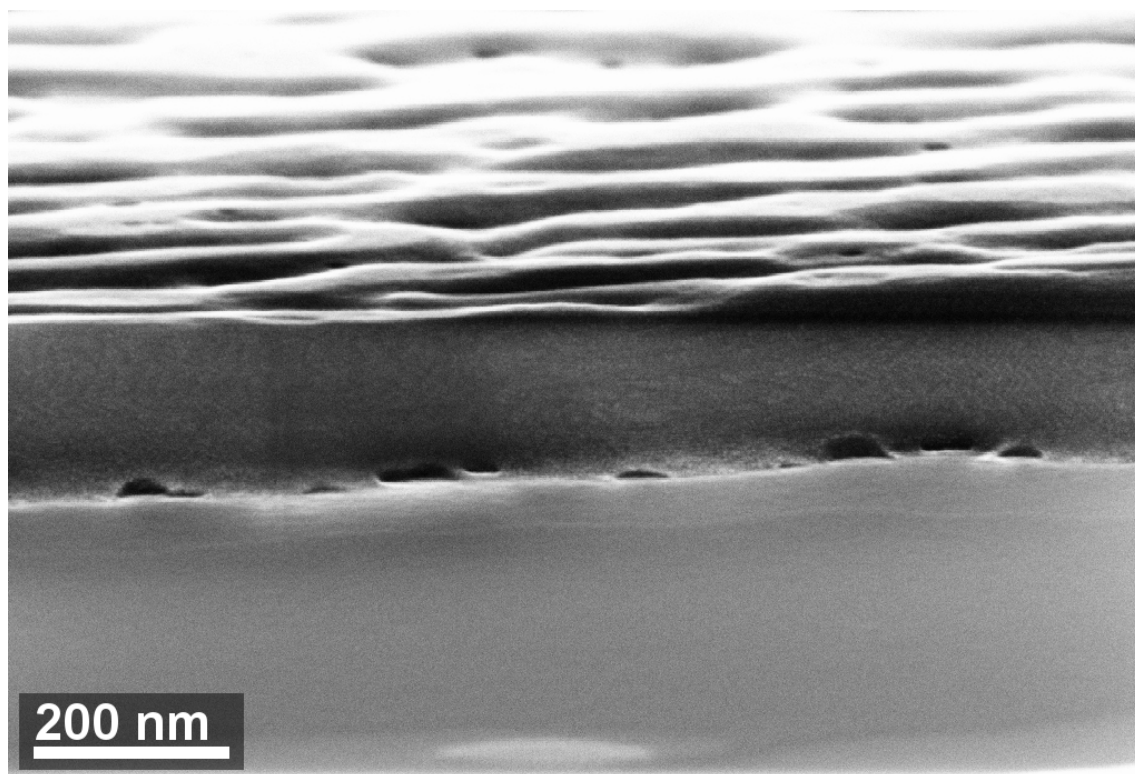


**Figure S11:** SEM image showing a cross sectional view of a GNP superlattice film from sample GNP1 deposited onto a silicon substrate.

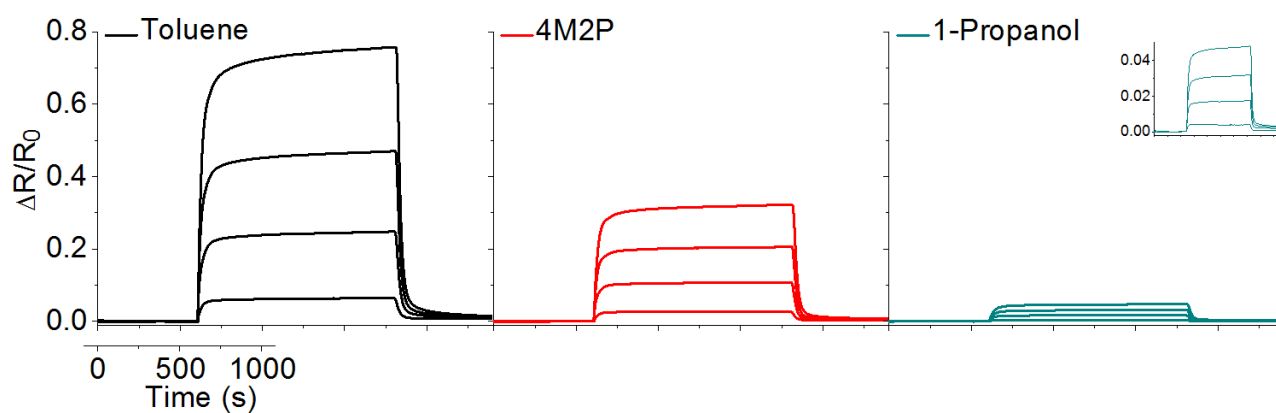


**Figure S12:** Chemiresistive responses of a GNP superlattice film, prepared from sample GNP1, to toluene (black), 4M2P (red) and 1-propanol (green) vapor. The vapor concentrations were 1000, 4000, 7000 and 10000 ppm.

### **3. Correlation of chemiresistive responses, sorption and swelling - Revisiting the chemiresistor model**

**Details on calculations of the density of GNP superlattice films, permittivity changes based on QCM and GISAXS data, and swelling based on QCM data**

#### **Geometrical model and calculation of the density of the GNP superlattice films**

GISAXS and TEM measurements revealed that the GNPs assemble into an fcc superlattice with  $\sim 2$  nm edge-to-edge interparticle spacing  $\delta$ . Scheme 2 (main document) shows a model of the superlattice based on the experimental data. Considering the length of the 1-dodecanethiol (DDT) ligands of  $1.8 \text{ nm}^{\text{S1}}$  in its fully extended conformation the interparticle distances of  $\sim 2$  nm (see Table 1, main document) indicate that the ligands interdigitate significantly. Thus, an fcc lattice is formed by spheres with a radius  $r_{\text{eff}}$ , comprising the gold core radius  $D/2$  plus half the interparticle distance, i.e.  $\delta/2$ . These spheres occupy 74% of the total superlattice volume. The remaining 26% of the volume are octahedral and tetrahedral interstitial sites into which the alkyl residues of the ligands extend by  $\sim 0.8$  nm. Therefore, superlattices formed by DDT-stabilized GNPs with a gold core diameter of  $\sim 4$  nm are expected to have no free volume within the tetrahedral sites. After subtracting the length of the alkyl residues extending into the octahedral sites, cavities with a diameter of  $\sim 0.6$  to  $0.7$  nm are expected. This is similar to experimentally obtained intermolecular spacings ( $\sim 0.5$  to  $\sim 0.7 \text{ nm}$ )<sup>S2-5</sup> in liquid alkanes. Thus, in our model we assume that the superlattice volume is completely filled by the gold cores and liquid 1-dodecanethiol. Accordingly, the density ( $\rho_{\text{sl}}$ ) of the GNP superlattice films and the volume ( $V_{\text{DDT}}$ ) filled by DDT were calculated as detailed below:

$$\rho_{sl} = n_{Au} + n_{DDT} \quad \text{Equation S 1}$$

with

$$n_{Au} = f_{Au} \cdot \rho_{Au} \quad \text{Equation S 2}$$

$$n_{DDT} = f_{DDT} \cdot \rho_{DDT} \quad \text{Equation S 3}$$

$$f_{Au} = \frac{r^3}{r_{eff}^3} \cdot 0.74 \quad \text{Equation S 4}$$

$$f_{DDT} = 1 - f_{Au} \quad \text{Equation S 5}$$

$$r_{eff} = r + \frac{\delta}{2}$$

$$V_{DDT} = (1 - f_{Au}) \cdot V_{sl} \quad \text{Equation S 6}$$

$n_{Au}$ : mass/volume fraction of gold

$n_{DDT}$ : mass/volume fraction of DDT

$f_{Au}$  respectively  $f_{DDT}$ : volume/volume fraction of gold respectively DDT

$\rho_{DDT}$ : density of DDT (0.845 g/cm<sup>3</sup>)

$\rho_{Au}$ : density of gold (19.32 g/cm<sup>3</sup>)

$r$ : radius of the gold cores (from TEM measurements)

$\delta$ : interparticle edge-to-edge distance obtained by subtracting the TEM-diameter of the gold cores from the center-to-center nearest neighbor distance determined by GISAXS

$V_{sl}$ : volume of the GNP superlattice

## Calculation of the permittivity

The permittivity of the analyte swollen ligand matrix  $\epsilon_{sw}$  was estimated as the volume-weighted average of the permittivity of the analyte and DDT<sup>S6,S7</sup>:

$$\epsilon_{sw} = f_{ana} \cdot \epsilon_{ana} + (1 - f_{ana}) \cdot \epsilon_{DDT} \quad \text{Equation S 7}$$

with

$\epsilon_{ana}$ : permittivity of the analyte

$\epsilon_{DDT}$ : permittivity of DDT

$f_{ana}$ : volume/volume fraction of the analyte within the organic matrix.  $f_{ana}$  was obtained from QCM data ( $f_{ana,qcm}$ ) or it was calculated from the swelling determined by GISAXS ( $f_{ana,gis}$ ).

### - Calculation of $f_{ana,qcm}$ based on QCM data:

$$f_{ana,qcm} = \frac{V_{ana,qcm}}{V_{DDT} + V_{ana,qcm}} \quad \text{Equation S 8}$$

$$V_{ana,qcm} = \frac{\rho_{sl} \cdot V_{sl} \cdot \frac{\Delta m}{m}}{\rho_{ana}} \quad \text{Equation S 9}$$

$f_{ana,qcm}$ : volume/volume fraction of the analyte within the ligand matrix

$V_{ana,qcm}$ : volume of sorbed analyte within the GNP film

$m$ : mass of the GNP film determined by QCM measurements

$\Delta m$ : mass increase upon sorption of solvent determined by QCM measurements

$\rho_{ana}$ : density of the analyte (toluene: 0.87 g/cm<sup>3</sup>, 4-methyl-2-pentanone: 0.80 g/cm<sup>3</sup>,

1-propanol: 0.80 g/cm<sup>3</sup> at 20 °C)

The permittivity of the analyte swollen ligand matrix based on QCM data is referred to as  $\epsilon_{sw,qcm}$ .

- **Calculation of  $f_{\text{ana,gis}}$  based on GISAXS data:**

Assuming isotropic swelling of the spheres with  $r_{\text{eff}}$ , the relative volume increase of the ligand shell (with initial thickness  $\delta/2$ ) upon analyte sorption is equal to the relative volume increase of the entire ligand matrix.

$$f_{\text{ana,gis}} = \frac{V_{\text{ana,gis}}}{V_{\text{eff,DDT}} + V_{\text{ana,gis}}} \quad \text{Equation S 10}$$

$$V_{\text{ana,gis}} = \frac{4}{3}\pi \left( r_{\text{eff}} + \frac{\Delta\delta}{2} \right)^3 - V_{\text{eff}} \quad \text{Equation S 11}$$

$$V_{\text{eff}} = \frac{4}{3}\pi r_{\text{eff}}^3 \quad \text{Equation S 12}$$

$$V_{\text{eff,DDT}} = V_{\text{eff}} - \frac{4}{3}\pi r^3 \quad \text{Equation S 13}$$

$f_{\text{ana,gis}}$ : volume/volume fraction of the analyte in the ligand matrix.

$V_{\text{ana,gis}}$ : volume of sorbed analyte forming a shell around the particle with radius  $r_{\text{eff}}$ .

The permittivity of the analyte swollen ligand matrix based on GISAXS data is referred to as  $\varepsilon_{\text{sw,gis}}$ .

**Calculation of swelling  $\Delta\delta_{\text{qcm}}$  based on QCM data**

The relative volume increase of the ligand matrix upon analyte sorption obtained from QCM measurements is assumed to be equal to the relative volume increase of the ligand shell of a sphere with  $r_{\text{eff}}$ :

$$\frac{V_{\text{ana,qcm}} + V_{\text{DDT}}}{V_{\text{DDT}}} = \frac{V_{\text{ana,shell}} + V_{\text{eff,DDT}}}{V_{\text{eff,DDT}}} \quad \text{Equation S 14}$$

$$V_{\text{ana,shell}} = \left( \left( r_{\text{eff}} + \frac{1}{2}\Delta\delta_{\text{qcm}} \right)^3 - r_{\text{eff}}^3 \right) \frac{4}{3}\pi \quad \text{Equation S 15}$$

With this, the resulting interparticle distance change is:

$$\Delta\delta_{\text{qcm}} = 2 \left( \sqrt[3]{r^3 + \left(1 + \frac{V_{\text{ana,qcm}}}{V_{\text{DDT}}}\right) (r_{\text{eff}}^3 - r^3)} - r_{\text{eff}} \right)$$

Equation S 16

### Comparison of measured chemiresistive responses with responses calculated using the chemiresistor model

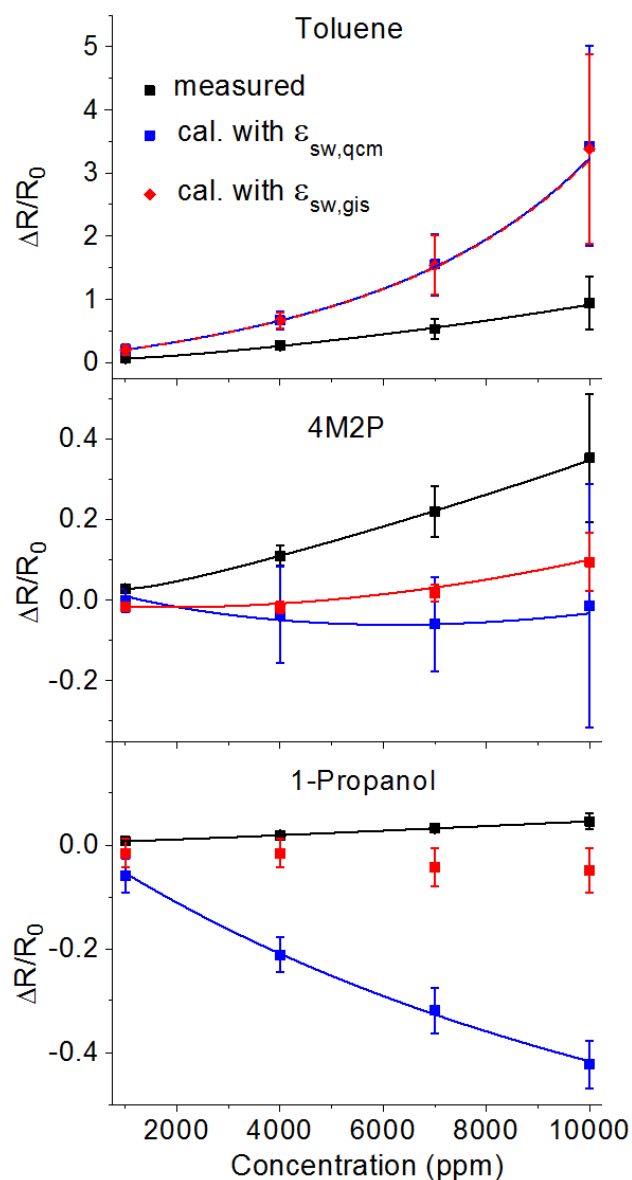


**Figure S13:** Measured and calculated chemiresistive responses according to eq.s 1 and 3 to toluene (top), 4M2P (middle) and 1-propanol (bottom) plotted vs. vapor concentration. For calculating the response amplitudes  $\Delta R/R_{0,\epsilon_{\text{qcm}}}$  (blue squares) and  $\Delta R/R_{0,\epsilon_{\text{gis}}}$  (red diamonds/squares) the GISAXS-measured swelling  $\Delta\delta$  (Figure 6) and the volume-weighted average permittivity of the analyte swollen ligand matrix,  $\epsilon_{\text{sw,qcm}}$  or  $\epsilon_{\text{sw,gis}}$  respectively were used.  $\epsilon_{\text{sw,qcm}}$  and  $\epsilon_{\text{sw,gis}}$  were calculated based either on QCM or GISAXS data, respectively, and using  $\epsilon_{\text{DDT}} = 2.0$ . The data points represent averages obtained from three films prepared using the GNP samples GNP1, GNP2 and GNP3. The individual data sets are shown in Figure S10.

The curves fitted to the data (solid and dashed lines) in Figure 11 (main document) and Figure S13 serve as guide to the eye and were generated using the chemiresistor model based on eq.s 1 and 3, which combined give the following equation:

$$\Delta R/R_{0,\text{cal}} = e^{\beta\Delta\delta} \cdot e^{\left[ \frac{e^2}{8\pi\epsilon_0} \left( \frac{1}{\epsilon_{\text{sw}}} \left( \frac{1}{r} - \frac{1}{r+\delta+\Delta\delta} \right) - \frac{1}{\epsilon_{\text{DDT}}} \left( \frac{1}{r} - \frac{1}{r+\delta} \right) \right) \right] / kT} - 1 \quad \text{Equation S 17}$$

For the blue and the red graphs  $\epsilon_{\text{sw}}$  and  $\Delta\delta$  were obtained from linear fit-functions obtained by plotting  $\epsilon_{\text{sw}}$  and  $\Delta\delta$  vs. vapor concentration. In the case of toluene  $\Delta\delta$  was obtained from a monoexponential fit-function (see Figure 6). The black solid lines represent fits to the measured chemiresistive responses based on eq. S 17. For 1-propanol the fit to the  $\Delta R/R_{0,\text{egis}}$  data was omitted due to scattering of the GISAXS data.

## References

- S1 C. D. Bain, E. B. Troughton, Y.-T. Tao, J. Evall, G. M. Whitesides and R. G. Nuzzo, *J. Am. Chem. Soc.*, 1989, **111**, 321–335.
- S2 Z. Bochyński and H. Drozdowski, *Acta Phys. Pol. A*, 1995, **88**, 1089–1096.
- S3 G. W. Stewart, *Phys. Rev.*, 1928, **31**, 174–179.
- S4 W. C. Pierce, *J. Chem. Phys.*, 1935, **3**, 252–255.
- S5 A. Z. Golik, A. F. Skryshevskii and I. I. Adamenko, *Zh. Strukt. Khim.*, 1967, **8**, 900–905.
- S6 A. M. Kummer, A. Hierlemann and H. Baltes, *Anal. Chem.*, 2004, **76**, 2470–2477.
- S7 W. H. Steinecker, M. P. Rowe and E. T. Zellers, *Anal. Chem.*, 2007, **79**, 4977–4986.